RESEARCH ARTICLE

Efficient Methodology of the Coil Design for a Dynamic Wireless Charger

ALICIA TRIVIÑO [ID]**[1], JESUS SÁNCHEZ[1], AND ALBERTO DELGADO** [ID]**[2], (Member, IEEE)**
[1]Escuela de Ingenierías Industriales, Universidad de Málaga, 29071 Málaga, Spain
[2]Centro de electrónica industrial, Universidad Politécnica de Madrid, 28040 Madrid, Spain

Corresponding author: Alicia Triviño (atc@uma.es)

ABSTRACT Dynamic charging is a promising technology that will increase the use of electric vehicles with reduced battery requirements. Designing this type of system is more complex than for a static charger, and leads to a significantly higher demand of computational resources. First, the complex geometries of the coils do not allow analytical equations to be used, and FE tools must therefore be used instead. However, the Litz wire conductor used in these coils will pose a computational problem if it is not well modelled. The second difficulty is that these systems should be analysed with more potential relative positions between the coils, as misalignment is intrinsic in a dynamic charger. These two complications mean that the design process can greatly benefit from techniques that reduce the time taken to derive the coil parameters. This paper shows the feasibility of using an equivalent layer to model the Litz wire in a dynamic charging application, which significantly reduces the computational time of each iteration up to 20 times. As a consequence, the complete design process is faster and accurate. For this demonstration, we illustrate the design for a dynamic charger of a remote control car.

I. INTRODUCTION

Electric Vehicles (EVs) now offer a feasible and sustainable solution to mobility needs [1]. They provide two main advantages. First, they significantly reduce the harmful emissions associated with the fuel-based transport sector. Second, when their charges and discharges are properly managed, they can also help to integrate renewable energy sources by adding a great deal of flexibility to the grid operation [2]. Wireless chargers can be used when the vehicle is parked (Figure 1.a), when it has temporarily stopped (Figure 1.b) or even when it is being driven on a road (Figure 1.c). Dynamic charging occurs in this last scenario.

There are several cities where dynamic charging has already been tested. For instance, in some cities in South Korea under the OLEV project [3], in Malaga (Spain) through the Victoria project [4], in the city of Douai (France) with the FastinCharge project [5], and in Turin (Italy) through the

The associate editor coordinating the review of this manuscript and approving it for publication was Agustin Leobardo Herrera-May [ID].

Conductix-Wampfler project [6]. The Fabric project [7] and the Smartroad Gotland project [8] have also tested dynamic wireless charging and include real implementation. All of these research works have a high cost because coils and power electronics should be replicated to provide continuous dynamic charging along a section of the road.

Wireless charger designs are usually based on an iterative algorithm in which the parameters are decided after evaluating the performance of a set of potential configurations. The difference for each configuration may be the coil dimensions and number of turns, the compensation topology, etc. For each configuration, the bifurcation problem, the efficiency, and the maximum voltage or currents in the circuit are analysed to determine its feasibility [9]. The algorithms for dynamic charging should include more iterations as they have to evaluate the performance of the potential solutions for perfect alignment and a number of misalignment conditions. Moreover, each of these iterations requires even more computational time than in static charging, as the coil topology is more complex to enable it to cope with misalignment [10].

FIGURE 1. Charging scenarios in EV wireless chargers [13].

(a) Static   (b) Stationary   (c) Dynamic

FIGURE 2. Representation of (a) an equivalent area of two Litz wire conductors. (b) the equivalent layer that contains the two homogenized Litz wires in (a).

In fact, for simple coil structures, each iteration may be executed quickly as their self- and mutual inductances can easily be computed based on equations [11]. However, other typical structures for dynamic charging – such as DD, bipolar, or DDQ – usually need finite element (FE) methods to compute the self- and the mutual inductances. Due to the operational frequency of these chargers, Litz wire is commonly used to deal with the skin effect [12]. Modelling the exact configuration of Litz wire as a set of multiple strands is extremely time-consuming. Moreover, if this type of conductor is not properly integrated in the charger model, the computation time to derive the electrical parameters of the coupler can reach up to 20 minutes in each iteration based on an FEM model, or it may not even conclude.

Considering this drawback, in this paper we demonstrate the feasibility of using a simplification to compute the characteristics of the coils in a dynamic charger. This technique reduces the execution time of the FEM simulations while guaranteeing that the process is completed. The basis of the simplification consists in modelling an equivalent conductor for the Litz wire of the coils. The resulting reduction in the computation time makes this method particularly suitable for dynamic charging. Based on this method, we show the design of a low-cost prototype for dynamic charging.

The paper is structured as follows. Section II describes how the Litz wire is simplified for the FEM analysis carried out in this work. Section III describes a generic procedure for applying the model in the coil design of a dynamic charger. With this methodology, the coils are designed as described in Section IV. In Section V, we present the experimental setup and the results for the prototype. Finally, Section VI concludes the paper.

II. LITZ WIRE MODELLING TO ACCELERATE FEM SIMULATIONS

In this section, we make a brief overview of the Litz wire modelling that accelerates the 3D finite element simulation. This modelling was initially developed in [14], [15] for static applications. It is based on the fact that the Litz wire is sufficiently well twisted so that all the strands are subjected to the same H field and the same current density J. We can make this assumption based on the size of the coils in relation to the twisting length.

The skin effect of each strand can be defined as:
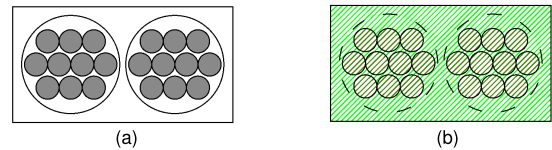
$$P_{se} = F_s R_{DC} I^2 \qquad (1)$$

where R_{DC} is the DC resistance of each strand, I is the peak current that circulates through the conductors, and F_s is a function based on Bessel's equation and is defined in [14].

On the other hand, the proximity magnetic losses of each strand can be defined as:

$$P_{pe} = \frac{G_p}{\sigma} H^2 \qquad (2)$$

where H is the magnetic field H that affects the conductors and G_p is based on Bessel-equation and is described in [14].

The diameter of the strands and their number make it impossible to simulate by brute force using finite element tools. A homogenization process is then necessary to conduct FE simulations in software tools such as Ansys Maxwell [16] or COMSOL Multiphysics [17]. Figure 2 illustrates a winding composed of two Litz wire conductors that cannot be simulated directly using FE tools. In our method, it is replaced by an equivalent layer (Figure 2) that keeps the same energy and magnetic and electrical losses of the actual winding, but the mesh is relaxed allowing the 3D fast FE simulations with similar results to characterize the coils. Thus, it is necessary to define the parameters of the equivalent layer. According to our proposal, we should set the following three parameters for the equivalent layer: σ_l, μ_l' and μ_l'', which are computed as follows.

The conduction losses of the equivalent layer can be calculated using:

$$P_{se} = \frac{1}{2} \int_v \sigma_l \overrightarrow{E}^2 dv \qquad (3)$$

Additionally, the losses due to the external magnetic field can be described by the magnetic losses of the layer using:

$$P_{pe} = \frac{1}{2} \int_v \mu_l'' \omega \overrightarrow{H}^2 dv \qquad (4)$$

By equalizing (1) and (3), it is possible to obtain a homogeneous conductivity for the equivalent layer [14] as:

$$\sigma_l = \frac{N_{turns} N_{strands}}{2 A_l F_s(\gamma) R_{DC}} \qquad (5)$$

On the other hand, equalizing (1) and (3), we can obtain the homogeneous imaginary part of the complex permeability that describes the proximity losses [14]:

$$\mu_l'' = \frac{2 N_{turns} N_{strands} G_p(\gamma)}{\sigma \omega \mu_0 A_l} \qquad (6)$$

Then, using the Kramers-Kronig relation [14], the real part of the complex permeability is obtained:

$$\mu_l' = \frac{2}{\pi} \int_0^\infty \frac{\mu_l''(x)x}{x^2 - \omega^2} dx + \mu_{cte}' \qquad (7)$$

where γ is defined by $d/\sqrt{2}\delta$, $N_{strands}$ is the number of strands in the Litz wire conductor, N_{turns} is the number of Litz wire conductors in the winding, A_l is the area of the equivalent layer that occupies one turn, μ_{cte}' is a value that ensures that the real permeability of the equivalent layer is 1 in low frequency.

When applying this modelling to dynamic charging, we can benefit from a more efficient design process for the inductive links. In dynamic charging, further aspects must be taken into account that are not considered in static charging. For example, it is necessary to analyse misalignment problems due to the car being misaligned on the road and being in continuous movement. The proposed procedure is also valid for other coil topologies, with multiple receivers as the ones described in [18] or in [19].

III. DESIGN PROCESS FOR A DYNAMIC WIRELESS CHARGER

The coupled coils are a key element in inductive-based wireless chargers. Their design must fulfil several requirements such as low cost, efficient power transmission, non-radiation to the non-objective regions and coupling with misalignment. The degree to which this last requirement must be satisfied determines the coil structure that the application should use. Static chargers may include a mechanism to control or reduce the misalignment condition when the power transfer is carried out, so they could opt for simple coil topologies such as circular or rectangular coils as shown in Figure 3.a and Figure 3.b. However, for those applications where misalignment may be more severe, particularly for dynamic charging, more complex coil structures are necessary. Nowadays, two coil structures are predominantly used for dynamic chargers. They are DD and DDQ coils, which are represented in Figure 3.c and Figure 3.d. In DD coils, which were used in [20], [21], the two equal D-shaped sub-coils are connected in parallel with a shared side. DD quadrature, or **DDQ**, which was used in [10], [22], is built with two independent windings. The first winding follows the DD geometry. The second coil, referred to as the quadrature coil, is built overlapping half of the area of each D component. This topology provides great flexibility to cope with misalignments and interoperability. However, when this type of coil is used, the power electronics and their control become more complex, as there are two subsystems to control [23]. To illustrate the proposed algorithm, we will analyse how a dynamic wireless charge should be designed using DD-coils. Nevertheless, the approach is also valid for other complex topologies, which will also benefit from the shorter design time.

For a DD-coil, the design variables that have the greatest influence on the coupling of the DD coils according to [21] are: coil width and length, distance between coils,
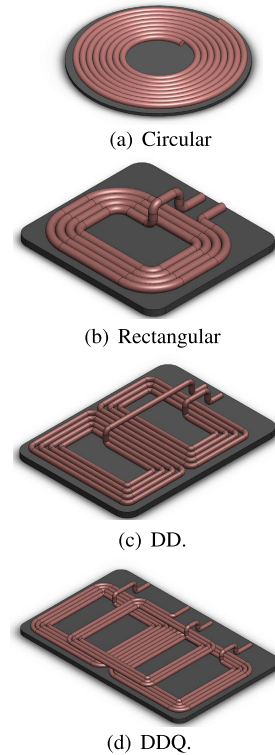

(a) Circular

(b) Rectangular

(c) DD.

(d) DDQ.

FIGURE 3. Coil topologies.

and the number of turns and pitch of the coils. Taking into account the coil parameters that must be decided in the design process, we should follow an iterative algorithm to determine their optimum combination. Some iterative algorithms are proposed in other design algorithms for static wireless chargers [24], but we include two main changes. First, for each potential configuration, the equivalent parameters of the Litz wire are obtained. As we explained in the previous Section, this simple computation clearly shortens the simulation time. Second, we have incorporated the need to analyse the charger's performance under certain misalignment conditions. In this way, we aim to improve the design for the complete conditions in which the dynamic charge occurs.

Figure 4 illustrates the proposed algorithm. For each dimension of the primary coil, we must determine the electrical parameters L_1, R_1 and Q_1 which stand for the self-inductance, the internal resistance and the quality factor of the primary coil. Instead of simulating the complex coil including its Litz wire winding, complex coil geometries with the equivalent-layer simplification are used. To do so, we will determine the equivalent parameters to conduct the simplified simulation based on the model described previously in an FE tool. To perform this step, we need to compute the features of the equivalent layer of the primary coil, that is, σ_{l1}, μ_{l1}' and μ_{l1}''. Similarly, for each configuration of the secondary coil geometries, we also compute its self-inductance, resistance and quality factor (L_2, R_2 and Q_2 respectively). For this computation, we first determine the parameters σ_{l2}, μ_{l2}' and μ_{l2}'' to include them in the equivalent model for the FE tool.

When we analyse the electrical parameters of the coils, we can determine whether a potential configuration of both coils is valid. In particular, to avoid bifurcation, some restrictions are imposed on the quality factors [25]. Using a specific combination of dimensions for the primary and secondary coils, we determine the mutual inductance for the inductive link with no misalignment, with a horizontal misalignment of 30%, and with one of 50%. We then design the compensation system. In the specific case of a Series-Series compensation and no misalignment, the values for the primary and the secondary capacitors (C_1 and C_2 respectively) are:

$$C_i = \frac{1}{\omega_o^2 L_i} \tag{8}$$

where ω_O corresponds to the operational angular frequency and $i \in \{1, 2\}$.

Once these capacitors are computed, we can derive the efficiency of the charger for the three operational conditions we want to test (no misalignment, 30% misalignment and 50% misalignment). These efficiencies (η_0, η_{30} and η_{50}) can be computed according to Equation 9 where j is 0, 30 and 50 respectively. The difference in these computations depends on the values of the mutual inductances (M_0, M_{30} and M_{50}).

$$\eta_j = \frac{R_L}{R_1 \left(\frac{R_2+R_L}{\omega_o M_j} \right)^2 + R_2 + R_L} \tag{9}$$

In the previous equation, R_L is the load resistance, i.e. the battery resistance (R_{bat}) perceived at the input of the secondary rectifier, as expressed in Equation 10. More details about the computation of the efficiency can be found in [9].

$$R_L = \frac{8R_{bat}}{\pi^2} \tag{10}$$

When all the feasible solutions have been identified, the algorithm evaluates them according to certain criteria (e.g. stability, cost, size, weight, etc.). Using this evaluation, the engineer decides the best option to implement. It can be observed that the algorithm is based on two nested loops. Thus, if the number of dimensions tested for the primary coil is N_1 and the number of dimensions considered for the secondary coil is N_2, the algorithm must execute $N_1 * N_2$ iterations with three sets of computations for each, according to the three misalignment conditions. The goal of this paper is to reduce the computational time of each iteration with the method proposed in the previous section.

IV. COIL DESIGN FOR A REMOTE CONTROL CAR

To illustrate our proposed design procedure, we developed a wireless charger for a High Speed Storm Remote Control Car, 1:12 Scale, as shown in Figure 5. The model is equipped with a 7.4 V 1500 mAh lithium-ion battery, with a charging time of two hours. The dimensions of the vehicle base, shown in Figure 6, must be taken into account when positioning the receiver coil.

Taking the space restrictions into account, we identified three potential configurations for the receiver coil and seven
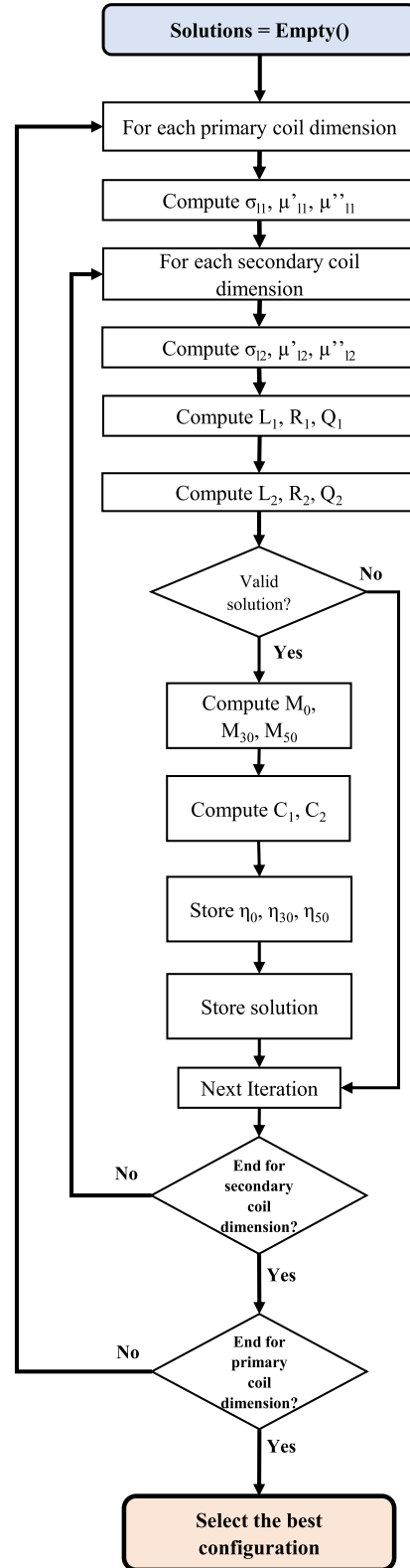

FIGURE 4. Flowchart of the proposed algorithm for designing the coils in dynamic chargers.

for the transmitter coil. Simplifying the Litz wire using a round solid conductor, it will take approximately 21 hours to evaluate the 21 combinations for the three misalignment
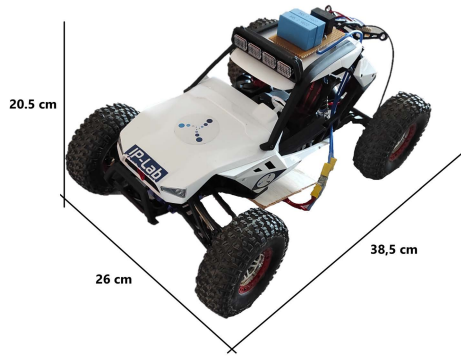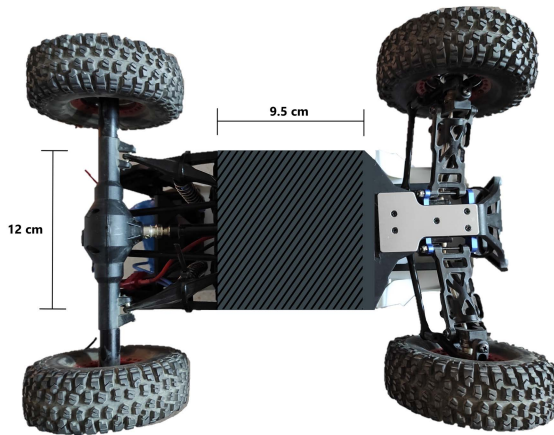
FIGURE 5. Car model general dimensions.

FIGURE 6. Car base dimensions.

conditions (each iteration takes nearly 20 minutes in a conventional PC) and the power losses must be computed analytically [26]. Due to the huge mesh used, some simulations may not even conclude. Thus, it is necessary to incorporate a simplified model such as the one described in this paper. Since each simulation using the equivalent layer with homogeneous parameters will be conducted in a few minutes and the power losses will be obtained directly, it is possible to reduce the time by almost 20 times. Its application is explained next.

A. APPLICATION OF THE EQUIVALENT LAYER TO THE COIL MODELLING

The electrical and magnetic properties of the equivalent layer are calculated according to the Litz wire used. Specifically, the main parameters to be considered are the number of strands, the diameter of each strand, and the diameter of the bundle. The number of turns and the area occupied by the winding are also important; however, those parameters will change for each configuration. The set of parameters for calculating the properties of the equivalent layer is shown in the Table 1.

When analysing the different cases, the number of turns and the area of the winding will change for the different coil configurations generated. However, the electrical and

TABLE 1. Characteristics of the Litz wire used in the model.

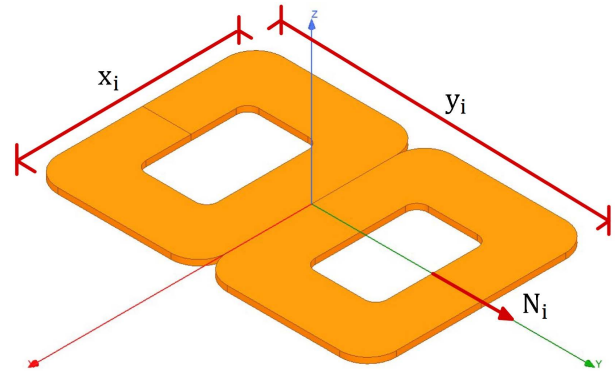|	
Copper conductivity (MS/m)	5.8
Relative magnetic permeability of copper	0.99999
Vacuum permeability (H/m)	$4\pi \cdot 10^{-7}$
Strand number	91
Strand diameter (mm)	0.2
Bundle diameter (mm)	2
Operating Frequency (kHz)	85

FIGURE 7. Coil dimensions.

magnetic properties of the equivalent layer model of Litz wire depend on the number of turns to be used in the coils.

To facilitate the design process, and since the equivalent parameters are proportional to the area of the layer and number of turns in the layer, it is possible to calculate the conductivity and complex permeability for the Litz wire for one conductor. The equivalent layer parameters will then be computed as:

$$\sigma_l = \frac{N_{turns}}{A_l}\sigma_{lw} \qquad (11)$$

$$\mu_l'' = \frac{N_{turns}}{A_l}\mu_{lw}'' \qquad (12)$$

where σ_{lw} and μ_{lw}'' are the properties for one Litz wire conductor. For our particular implementation at 85 kHz, σ_{lw} and μ_{lw} are $5.3 \cdot 10^7$ and $1 + j0.0896$ respectively.

Different configurations of the inductive link are simulated in Ansys Maxwell using the 3D model shown in Figure 7. The parameters x_i and y_i are the dimensions of the coils and N_i corresponds to the number of turns. Subindex $i = 1$ refers to the transmitter coil, while the use of $i = 2$ relates to the receiver coil.

The primary and secondary coils present some differences due to limitations in the the number of turns and in the dimensions. The transmitter coil was modelled for the following three coil dimensions:

- Model A was designed with $y_1 = 120$ mm and $x_1 = 80$ mm with three potential turns so $N_1 \in \{10, 12, 14\}$.
- Model B results in larger coils, as the dimensions are $y_1 = 150$ mm and $x_1 = 100$ mm with $N_1 \in \{12, 14, 16\}$.

TABLE 2. Self-inductances and resistances of the transmitter coil models.

Model	Dimensions (mm^2)	N_1	L_1 (μH)	R_1 (mΩ)
A.1.10		10	6.98	31.60
A.1.12	120 x 80	12	8.38	37.29
A.1.14		14	9.28	41.73
B.1.12		12	12.99	48.17
B.1.14	150 x 100	14	15.61	56.41
B.1.16		16	17.00	61.00
C.1.12	180 x 120	12	19.46	64.94

TABLE 3. Self-inductances and resistances of the receiver coil models.

Model	Dimensions (mm^2)	N_2	L_2 (μH)	R_2 (mΩ)
A.2.10		10	6.98	31.60
A.2.12	120 x 80	12	8.38	37.29
A.2.14		14	9.28	41.73

- Model C is even larger, in order to analyse the importance of the dimensions of the primary coil with $y_1 = 180$ mm and $x_1 = 120$mm with $N_1 = 12$.

The particular configurations for the seven topologies tested for the transmitter are detailed in Table 2. We specify the self-inductance and resistance obtained through the simulations for each of the models. When we analysed the results, we identified an increase in both inductance and resistance due to the increased size of the coils and number of turns. Subsequently, we carried out simulations to observe how these models behave with the receiver coil models.

With regard to the receiver, the coil was modelled for a single dimension, with the intention of taking advantage of the maximum space available in the base of the vehicle. Thus, $y_2 = 120$ mm and $x_2 = 80$ mm. In addition, analogously to the previous case, this coil was modelled for a different number of turns, i.e. $N_2 \in \{10, 12, 14\}$. The self-inductance and AC resistance obtained from the FE tool can be seen in the following Table 3. In this case, there is also an increase in the self-inductance when the number of turns increases due to the larger transmission surface of the coil.

B. ELECTRICAL ANALYSIS

Using the flowchart presented in Figure 4 and the equations of a Series-Series wireless charger, we derived the quality factors and the capacitors for each of the 17 configurations tested. They are summarized in Table 4.

We then computed the mutual inductances in the case of no misalignment (Figure 8) and 30% and 50% horizontal misalignment (Figures 9.a and 9.b respectively). When working with dynamic charging, it is usual to analyse wireless charging for different misalignment conditions [27]. In Table 4, these parameters are included. When we focus on the values obtained in the case of no misalignment, we find that all the configurations show an efficiency higher than 75%. In certain cases, where the transmitter coil has the largest dimension, an efficiency of over 85% is obtained, with a maximum
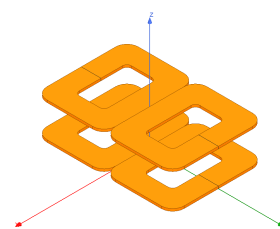

FIGURE 8. Model without misalignment in Ansys Maxwell.

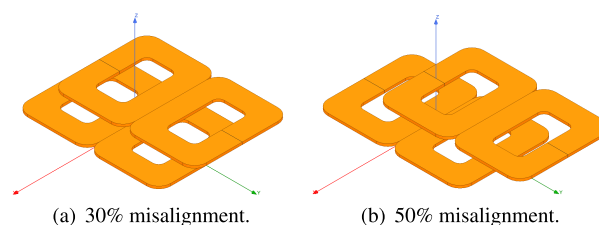(a) 30% misalignment. (b) 50% misalignment.

FIGURE 9. Models with misalignment in Ansys Maxwell.

value of 89.61% for the configuration whose transmitter and receiver coils have the largest dimensions and number of turns of all those simulated. These configurations also involve a higher cost due to the material used in the number of turns of the primary and secondary coils. However, their efficiency is considerably higher and so they are a very good option.

When we analyse the results in Table 4 for a misalignment of 30%, we find that there is a significant reduction in the efficiency of the system. We observe values ranging from 70% for the configurations with the smallest transmitter coils to 85% for the largest ones. For the given misalignment, the efficiencies are still acceptable. Regarding the efficiency for a misalignment of 50%, there is a very significant reduction in efficiency for coils whose dimension is $120 \times 80\ mm^2$. Values of around 50% are obtained for these, which is a very low efficiency figure. However, for coils with a larger dimension of $150 \times 100\ mm^2$, the efficiency is around 75%,

TABLE 4. Simulated mutual inductance for the three misalignment conditions.

| Transmitter	Receiver	M_0 (μH)	M_{30} (μH)	M_{50} (μH)	η_0 (%)	η_{30} (%)	η_{50} (%)	E/L
A.1.10	A.1.10	1.35	1.08	0.74	76.32	67.84	49.57	10.42
A.1.10	A.1.12	1.48	1.18	0.80	79.31	71.38	53.35	10.16
A.1.10	A.1.14	1.55	1.27	0.88	80.65	74.02	57.93	9.83
A.1.12	A.2.12	1.63	1.31	0.89	79.74	72.06	54.52	9.97
A.1.12	A.2.14	1.72	1.39	0.95	81.29	74.29	57.62	9.68
A.1.14	A.2.14	1.81	1.45	0.99	81.13	73.86	56.90	9.21
B.1.12	A.2.10	2.32	1.92	1.41	85.97	80.86	69.88	8.60
B.1.12	A.2.12	2.55	2.12	1.55	87.90	83.65	73.55	8.62
B.1.12	A.2.14	2.67	2.24	1.64	88.70	84.96	75.55	8.37
B.1.14	A.2.10	2.57	2.12	1.55	86.50	81.54	70.53	8.12
B.1.14	A.2.12	2.83	2.34	1.71	88.39	84.18	74.27	8.15
B.1.14	A.2.14	2.98	2.47	1.80	89.27	85.44	76.06	7.94
B.1.16	A.2.10	2.71	2.22	1.61	86.81	81.79	70.49	7.75
B.1.16	A.2.12	3.00	2.45	1.77	88.76	84.40	74.10	7.79
B.1.16	A.2.14	3.16	2.60	1.87	89.61	85.66	76.02	7.59
C.1.12	B.1.12	4.22	3.88	2.85	94.09	93.27	89.00	7.36
C.1.12	A.2.12	2.95	2.64	1.88	89.87	87.87	79.23	8.50
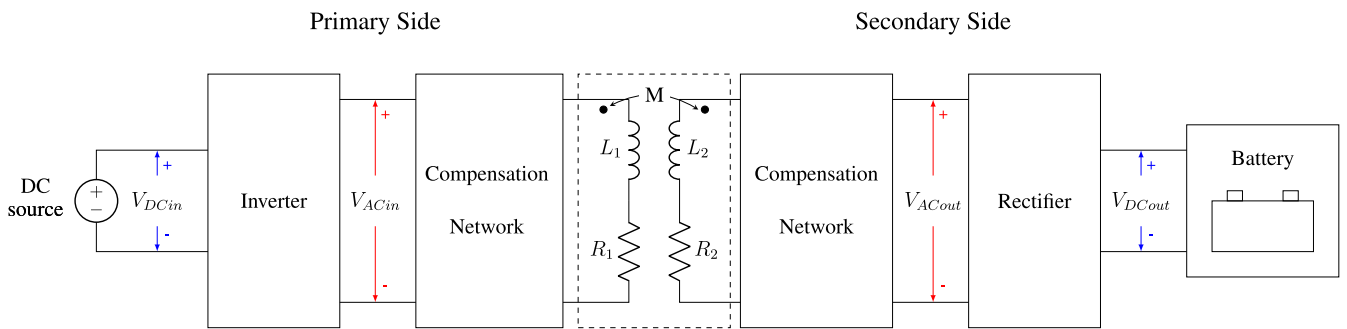
FIGURE 10. Structure of a wireless charger for electric vehicles with power converters.

which could be considered acceptable. This is due to the fact that the transmitter coil is larger than the receiver coil, which favours the transmission of the electromagnetic flux, providing a better coupling coefficient and therefore a better mutual inductance and higher induced voltage.

Knowing the efficiencies of each case, an efficiency-to-length ratio (E/L) is established as a figure of merit. This is computed as the efficiency divided by the sum of the length of the primary and secondary coils. Since dynamic charging involves replicating several primary coils to provide energy while the vehicle is moving, its length will have an impact on its cost. In addition, longer coils on the secondary side weigh more, which is a disadvantage. The E/L parameter is included in Table 4 to help identify the optimal configuration. It is also plotted in Figure 11.

In Table 4, we can see that the efficiency-cost ratio is better for models with smaller dimensions as they are efficient and cost less. However, in this case, it is not advisable to follow this indication exclusively because it is important for

the efficiency to be as high as possible, even if the cost increases. Studying the values of the total efficiency-length ratio for other configurations, we find that the efficiency of the different configurations of model B.1.16 is among the highest, but the efficiency-length parameter is the lowest; these configurations are therefore not the most suitable and are discarded. The same applies to the configurations of model B.1.14 and B.1.12. We thus chose a configuration with the primary coil model C.1.12. From this model, two options for the secondary coil are available, which differ mainly in the number of turns. If the efficiency-length parameter is analysed again, we find that the optimum configuration is the one with the secondary coil model A.2.12. The efficiency is slighter lower than for the alternative configuration, but the weight in this type of application must be minimised and the efficiency/length should be maximized. All things considered, the best configuration for the prototype of the electric vehicle charger consists of model C.1.12 as the primary coil and model A.2.12 as the secondary coil.
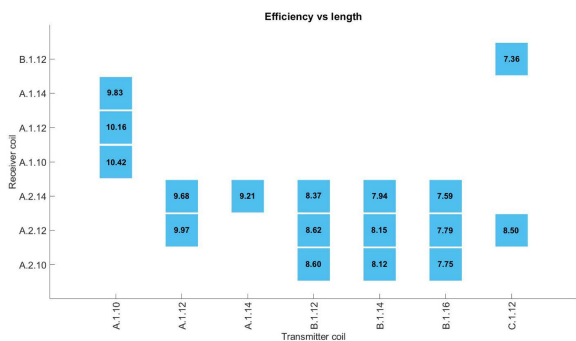
FIGURE 11. Efficiency vs length of the tested coils.

TABLE 5. Electrical parameters of the implemented coils.

Parameter	Simulated value	Measured value
L_1 (μH)	19.46	19.27
R_1 ($m\Omega$)	64.94	53.76
L_2 (μH)	8.38	8.81
R_2 ($m\Omega$)	37.29	34.41
M_0 (μH)	2.95	2.80
M_{30} (μH)	2.64	2.54
M_{50} (μH)	1.88	1.64

(a) Primary coil.　　　(b) Secondary coil.
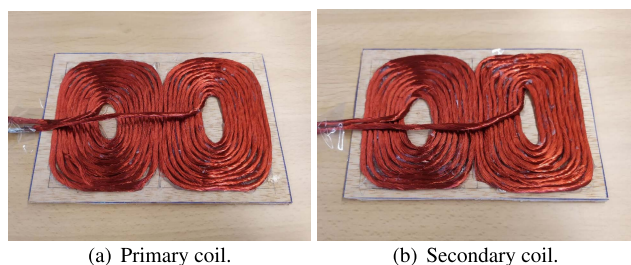
FIGURE 12. Coils built in the laboratory.

V. EXPERIMENTAL EVALUATION

The design process was validated by implementing the prototype in the aforementioned remote control car. The coils used are shown in Figure 12.

The electrical parameters of the coils we constructed were obtained using the LCR HM812 meter. They are summarized in Table 5. As can be seen in this table, the measurements we obtained in the laboratory are close to the theoretically simulated values. These results confirm that the simplified model can be used to design the coils, as described in this paper.

As shown in Eq. 8, we derived the value of the compensation systems for the coils used. Specifically, we found that the value of the primary capacitor should be 293 nF, and the secondary capacitor should have a value of 400 nF. When developing the prototype, power converters are inserted as shown in Figure 10. The full-bridge inverter is implemented with model KIT8020-CRD-8FF1217P-1 from CREE [28]. On the secondary side, a non-controllable rectifier is used to reduce the weight. The final implementation is shown in Figure 13.
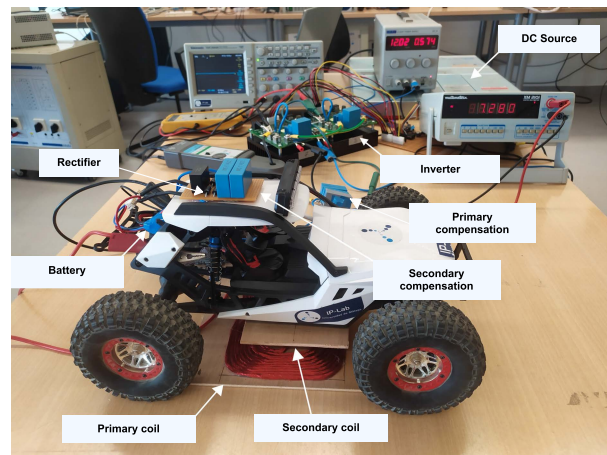

FIGURE 13. Implementation of the wireless charger in the vehicle.

Using the EV battery, we performed three sets of tests: when the EV presents (i) no misalignment; (ii) 30% misalignment; and (iii) 50% misalignment. The voltage and current signals were analysed on both the primary and secondary sides. The objective of the first test was to determine the behaviour of the charger when it is in the zone of maximum energy transfer, i.e. when there is no misalignment. When we analyse the voltage and current signals on the primary and secondary sides, represented in Figure 14, we find that there is little or no phase difference between the two signals on both the primary and the secondary sides.

After checking that the voltage and current signals were correct, we calculated the efficiency of the charger for a supply voltage of 10 V and a current of 3.65 A, giving an efficiency of 57.71%. We calculated DC efficiency considering the signals at the input of the inverter (V_{DCin}), and at the output of the rectifier (V_{DCout}. We determined AC efficiency from the signals at the output of the inverter (V_{ACin}) and at the input of the rectifier (V_{ACout}), according to Figure 10. When we analyse the signals represented in Figure 14, we find that AC efficiency η_0 is 95.23%.

For the second test, we moved the secondary coil horizontally by 3.5 cm to analyse how misalignment affects the charger. To do so, we analysed the voltage and current signals on the primary and secondary sides of the charger, represented in Figure 15. We observe that the phase difference between current and voltage increases on the primary side; as a result, the energy transfer is reduced and the charger is less efficient. The difference in the phase is considered when computing the active power. In this scenario, the efficiency η_{30} is 47.36%.

In this case, taking into account the misalignment produced, the power supply delivers a voltage of 6.9 V and a current of 5 A, while in the battery area a voltage of 7.1 V and a current of 1.16 A is obtained. Using these values, we obtain an efficiency of 23.87% in a direct current and an efficiency of 47.36% in an alternating current.
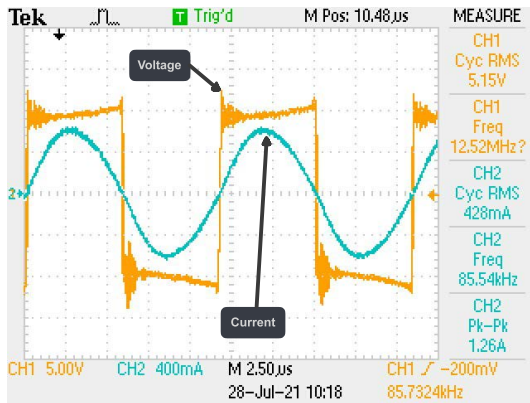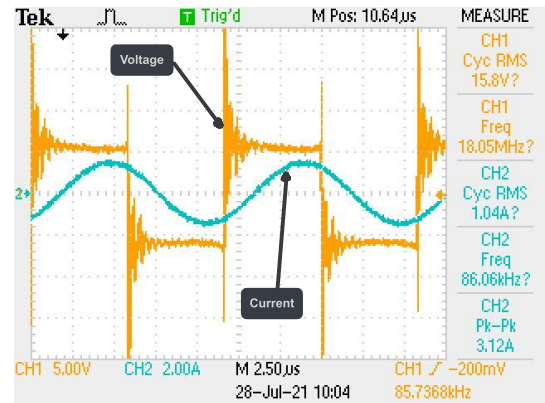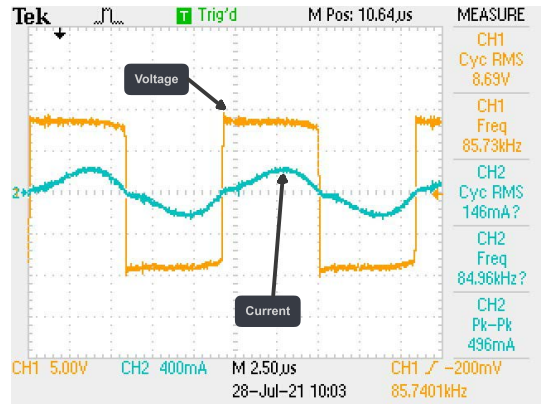
(a) Primary voltage and current.
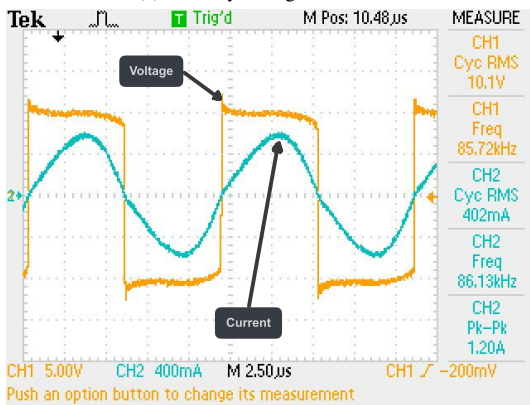
(b) Secondary voltage and current.

FIGURE 14. Wireless charge test without misalignment.

(a) Primary voltage and current.

(b) Secondary voltage and current.

FIGURE 15. Wireless charge test with a misalignment of 30%.

**TABLE 6.** Efficiencies obtained according to the distance.

Distance (cm)	DC Efficiency	AC Efficiency
0	57.71%	95.23%
3.5	23.87%	47.36%
7.5	45.40%	83.86%

In the last test, we displaced the secondary coil by 7.5 cm with respect to the primary coil in order to determine whether the charger's behaviour improves or worsens in relation to the previous scenario. Analysing the voltage and current signals, which can be seen in Figure 16, the phase difference between the voltage and current decreases in the primary coil, while both signals in the secondary coil remain in phase. As the phase difference between the two signals decreases, the energy transfer improves and the efficiency of the charger increases, reaching an efficiency in direct current of 45.40% and an efficiency in alternating current (η_{50}) of 83.86%. All the efficiencies are summarized in Table 6. Due to the low power managed in this application, the non-idealities of the components clearly impact on the diminution of the efficiency if we compare it with high-power applications.

As can be seen during the battery test, for a misalignment of 30%, there is a drop in efficiency of around 47%, which is a greater reduction than we see with a misalignment of 50%. In fact, the efficiency for this latter scenario is almost

double the efficiency obtained for the previous case. DD coils usually behave in this way, so we can identify a misalignment range where the output power of the charger is zero. This is due to the fact that the magnetic field is cancelled for a specific range of relative positions of the secondary coil with respect to the primary coil, and therefore, there is no energy transfer. We experimentally derived the output power of the charger for a wide range of potential misalignments to verify that this occurs. Figure 17 shows the output power measured in the laboratory. When there is a horizontal displacement of between 40 and 60 mm, there is a zone where the power at the output of the charger is zero. We find that a low output power is obtained for a misalignment of 30%, whereas a misalignment of 50% does not result in such a severe loss of performance. These facts explain the relative difference in efficiency between the two positions tested.

In conclusion, we designed a valid prototype for dynamic charging based on a simplified model, as shown. Charging the vehicle at minimum speed is feasible, as the vehicle can travel 54 metres without needing to pass over another coil for a short period of time. This is because there is only a single coil available, whereas it is usual and most appropriate for the vehicle to pass over several contiguous coils during charging,
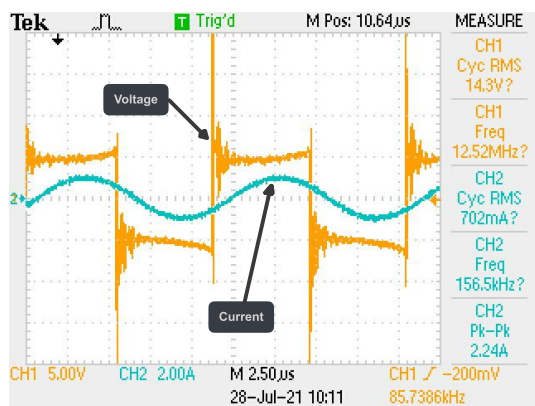
(a) Voltage and current in the primary
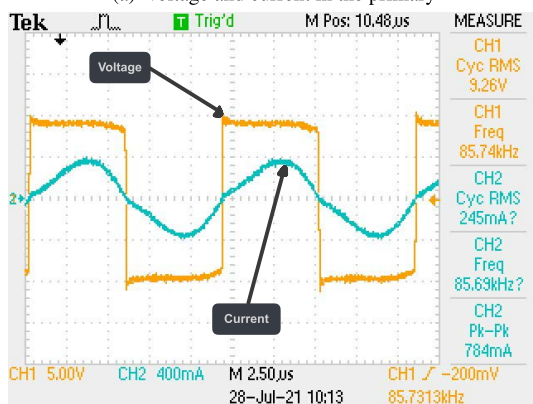
(b) Voltage and current in the secondary.

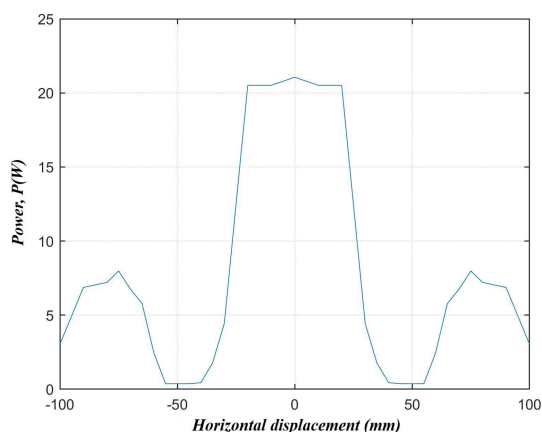**FIGURE 16. Battery load test with 50% misalignment.**

FIGURE 17. Power vs horizontal misalignment: zero power point.

allowing a longer charging period and thus a longer distance to the next charging zone.

VI. CONCLUSION

Dynamic charging is a promising technology that enables EVs to be charged while on the move. Several research topics such as coil design, power electronics and control are currently being studied in this field. Studies based on finite element modelling are often required, which makes the

design processes slow. In this paper, we study how to apply a simplified model for FEM tools in order to achieve a faster and more accurate design. We have applied the model to design and implement a dynamic charge prototype. With our simplified model, the simulations are 20 times faster than with a conventional method. The experimental results demonstrate the feasibility and convenience of using the simplified model, as the features measured are close to those derived with the modelling. With the prototype, we have achieved 95.2% of AC efficiency with no misalignment and 47.36% and 83.36% AC efficiencies for 30% and 50% misalignment respectively. We could identify the effects of the zero power point related to the DD coils.

REFERENCES

[1] R. R. Kumar and K. Alok, "Adoption of electric vehicle: A literature review and prospects for sustainability," *J. Cleaner Prod.*, vol. 253, Apr. 2020, Art. no. 119911.
[2] P. Sharifi, A. Banerjee, and M. J. Feizollahi, "Leveraging owners' flexibility in smart charge/discharge scheduling of electric vehicles to support renewable energy integration," *Comput. Ind. Eng.*, vol. 149, Nov. 2020, Art. no. 106762.
[3] A. Foote and O. C. Onar, "A review of high-power wireless power transfer," in *Proc. IEEE Transp. Electrific. Conf. Expo (ITEC)*, Jun. 2017, pp. 234–240.
[4] H. Bludszuweit, "Project Victoria—The first Spanish showcase for DWPT," presented at the FABRIC Conf. Presentation, Feb. 2016.
[5] *FastinCharge: Innovative Fast Inductive Charging Solution for Electric Vehicles*. Accessed: Feb. 1, 2021. [Online]. Available: https://cordis.europa.eu/project/id/314284/reporting/es
[6] Eltis. *Wireless Charging for Quiet and Clean Public Transport in Torino (Italy)*. Accessed: Jan. 22, 2021. [Online]. Available: https://www.eltis.org/discover/case-studies/wireless-charging-quiet-and-clean-public-transport-torino-italy
[7] *Fabric—Fabric EU Project*, Seven Framework Programme, Eur. Commission, Brussels, Belgium, 2018.
[8] *Home|Smartroad Gotland*, Trafikverket, Swedish Transp. Admin., Stockholm, Sweden, 2019.
[9] A. T. Cabrera, J. M. G. González, and J. A. Aguado, *Wireless Power Transfer for Electric Vehicles: Foundations and Design Approach*. Cham, Switzerland: Springer, 2020.
[10] Z. Zhang, H. Pang, C. H. T. Lee, X. Xu, X. Wei, and J. Wang, "Comparative analysis and optimization of dynamic charging coils for roadway-powered electric vehicles," *IEEE Trans. Magn.*, vol. 53, no. 11, pp. 1–6, Nov. 2017.
[11] A. Delgado, G. D. Capua, K. Stoyka, L. Shi, N. Femia, A. Maffucci, S. Ventre, P. Alou, J. Á. Oliver, and J. A. Cobos, "Self and mutual inductance behavioral modeling of square-shaped IPT coils with air gap and ferrite core plates," *IEEE Access*, vol. 10, pp. 7476–7488, 2022.
[12] D. Barth, B. Klaus, and T. Leibfried, "Litz wire design for wireless power transfer in electric vehicles," in *Proc. IEEE Wireless Power Transf. Conf. (WPTC)*, May 2017, pp. 1–4.
[13] A. Triviño, J. M. González-González, and J. A. Aguado, "Wireless power transfer technologies applied to electric vehicles: A review," *Energies*, vol. 14, no. 6, p. 1547, Mar. 2021.
[14] A. Delgado, G. Salinas, J. A. Oliver, J. A. Cobos, and J. Rodriguez-Moreno, "Equivalent conductor layer for fast 3-D finite element simulations of inductive power transfer coils," *IEEE Trans. Power Electron.*, vol. 35, no. 6, pp. 6221–6230, Jun. 2020.
[15] A. Delgado, G. Salinas, J. A. Oliver, J. A. Cobos, and J. Rodriguez-Moreno, "Equivalent parameters of round and litz wire conductors to obtain an equivalent layer to accelerate finite element simulations of wireless power transfer system," in *Proc. IEEE Energy Convers. Congr. Expo. (ECCE)*, Sep. 2018, pp. 7375–7379.
[16] *Ansys Maxwell*. Accessed: Nov. 8, 2021. [Online]. Available: https://www.ansys.com/products/electronics/ansys-maxwell
[17] *COMSOL Multiphysics*. Accessed: Nov. 8, 2021. [Online]. Available: https://www.comsol.com/comsol-multiphysics
[18] N. Mohamed, F. Aymen, M. Alqarni, R. A. Turky, B. Alamri, Z. M. Ali, and S. H. E. A. Aleem, "A new wireless charging system for electric vehicles using two receiver coils," *Ain Shams Eng. J.*, vol. 13, no. 2, Mar. 2022, Art. no. 101569.

[19] V.-B. Vu, J. M. Gonzalez-Gonzalez, V. Pickert, M. Dahidah, and A. Trivino, "A hybrid charger of conductive and inductive modes for electric vehicles," *IEEE Trans. Ind. Electron.*, vol. 68, no. 12, pp. 12021–12033, Dec. 2021.

[20] L. Xiang, Y. Sun, C. Tang, X. Dai, and C. Jiang, "Design of crossed DD coil for dynamic wireless charging of electric vehicles," in *Proc. IEEE PELS Workshop Emerg. Technol., Wireless Power Transf. (WoW)*. Piscataway, NJ, USA: Institute of Electrical and Electronics Engineers, May 2017, pp. 1–5.

[21] M. Budhia, J. T. Boys, G. A. Covic, and C.-Y. Huang, "Development of a single-sided flux magnetic coupler for electric vehicle IPT charging systems," *IEEE Trans. Ind. Electron.*, vol. 60, no. 1, pp. 318–328, Jan. 2013.

[22] Y. Li, J. Hu, T. Lin, X. Li, F. Chen, Z. He, and R. Mai, "A new coil structure and its optimization design with constant output voltage and constant output current for electric vehicle dynamic wireless charging," *IEEE Trans. Ind. Informat.*, vol. 15, no. 9, pp. 5244–5256, Sep. 2019.

[23] G. R. Nagendra, G. A. Covic, and J. T. Boys, "Determining the physical size of inductive couplers for IPT EV systems," *IEEE J. Emerg. Sel. Topics Power Electron.*, vol. 2, no. 3, pp. 571–583, Sep. 2014.

[24] J. Sallan, J. L. Villa, A. Llombart, and J. F. Sanz, "Optimal design of ICPT systems applied to electric vehicle battery charge," *IEEE Trans. Ind. Electron.*, vol. 56, no. 6, pp. 2140–2149, Jun. 2009.

[25] C.-S. Wang, G. A. Covic, and O. H. Stielau, "Investigating an LCL load resonant inverter for inductive power transfer applications," *IEEE Trans. Power Electron.*, vol. 19, no. 4, pp. 995–1002, Jul. 2004.

[26] R. Bosshard and J. W. Kolar, "Multi-objective optimization of 50 kW/85 kHz IPT system for public transport," *IEEE J. Emerg. Sel. Topics Power Electron.*, vol. 4, no. 4, pp. 1370–1382, Dec. 2016.

[27] N. Mohamed, F. Aymen, T. E. A. Alharbi, C. Z. El-Bayeh, S. Lassaad, S. S. M. Ghoneim, and U. Eicker, "A comprehensive analysis of wireless charging systems for electric vehicles," *IEEE Access*, vol. 10, pp. 43865–43881, 2022.

[28] A. Triviño-Cabrera, J. M. González-González, and J. A. Aguado, "Design and implementation of a cost-effective wireless charger for an electric bicycle," *IEEE Access*, vol. 9, pp. 85277–85288, 2021.

JESUS SÁNCHEZ received the B.Sc. degree in industrial technologies engineering and the M.Sc. degree in industrial engineering from the University of Malaga (UMA), Spain, in 2019 and 2021, respectively. He is currently working as a Project Engineer, developing projects for building installations.

ALICIA TRIVIÑO received the master's degree in telecommunication engineering and computer science engineering from the University of Malaga, Spain, in 2002 and 2008, respectively. Her thesis, which she defended, in 2007, focused on wireless networks. She currently holds a position as an Associate Professor at the University of Malaga. Since 2011, her research interests include wireless power transfer. In the field of electric vehicle wireless chargers, she has played an active role in designing and developing three prototypes, including features, such as bi-directionality and dynamic charging.

ALBERTO DELGADO (Member, IEEE) received the B.Sc. degree in electrical engineering from the University of Malaga (UMA), Spain, in 2016, and the M.Sc. and Ph.D. degrees in industrial electronics from the Polytechnic University of Madrid (UPM), in 2017 and 2021, respectively.

He became a Teaching Assistant at UPM, in 2019. His research interests include modeling of DC-DC converters for inductive power transfer systems and magnetic components for different applications, such as RFID communications and wireless charging and magnetic nano-materials and micro-materials. During his undergraduate studies, he was awarded honours on several occasions, and he achieved the Best Student of the Year Award.

• • •